SIAM/ASA J. UNCERTAINTY QUANTIFICATION
Vol. 3, pp. 873–896

Probabilistic Density Function Method for Stochastic ODEs of Power Systems with Uncertain Power Input*

P. Wang†, D. A. Barajas-Solano‡, E. Constantinescu§, S. Abhyankar§, D. Ghosh§, B. F. Smith§, Z. Huang‡, and A. M. Tartakovsky¶

Abstract. Wind and solar power generators are commonly described by a system of stochastic ordinary differential equations (SODEs) where random input parameters represent uncertainty in wind and solar energy. The existing methods for SODEs are mostly limited to delta-correlated random parameters, while the uncertainties from renewable generation exhibit colored noises. Here we use the probability density function (PDF) method, together with a novel large-eddy-diffusivity (LED) closure, to derive a closed-form deterministic partial differential equation (PDE) for the joint PDF of the SODEs describing a power generator with correlated-in-time power input. The proposed LED accurately captures the effect of nonzero correlation time of the power input on systems described by a divergent stochastic drift velocity. The resulting PDE is solved numerically. The accuracy of the PDF method is verified by comparison with Monte Carlo simulations.

Key words. uncertainty quantification, PDF method, swing equation, renewable energy

AMS subject classifications. 60H10, 60H30, 60H35, 65C20

DOI. 10.1137/130940050

1. Introduction.

In the near future, a significant portion of electricity generation in the U.S. may come from renewable sources. Contrary to production of conventional fossil fuels, production of renewable (i.e., wind and solar) energy typically exhibits spatio-temporal variations and is ubiquitously uncertain. Therefore, the increasing share of power generation from renewable sources poses a fundamental challenge to the existing power grid in its ability to cope with uncertainty in power generation. One way to address this challenge is to employ

*Received by the editors October 7, 2013; accepted for publication (in revised form) July 27, 2015; published electronically September 22, 2015. This work was supported by the Applied Mathematics Program within the U.S. Department of Energy Office of Advanced Scientific Computing Research as part of the Multifaceted Mathematics for Complex Systems project. Pacific Northwest National Laboratory is operated by Battelle for the U.S. Department of Energy under contract DE-AC05-76RL01830. This work was performed by employees of the U.S. Government or under U.S. Government contract. The U.S. Government retains a nonexclusive, royalty-free license to publish or reproduce the published form of this contribution, or allow others to do so, for U.S. Government purposes.

http://www.siam.org/journals/juq/3/94005.html

†Pacific Northwest National Laboratory, Richland, WA 99352. Current address: Beihang University, Beijing, China, 100191 (wang.peng@buaa.edu.cn).

‡Pacific Northwest National Laboratory, Richland, WA 99352 (david.barajas-solano@pnnl.gov, zhenyu.huang@pnnl.gov).

§Argonne National Laboratory, Argonne, IL 60439 (emconsta@mcs.anl.gov, abhyshr@mcs.anl.gov, ghosh@mcs.anl.gov, bsmith@mcs.anl.gov).

¶Corresponding author. Pacific Northwest National Laboratory, Richland, WA 99352 (alexandre.tartakovsky@pnnl.gov). This author's research was supported by the New Dimension Reduction Methods and Scalable Algorithms for Multiscale Nonlinear Phenomena project.

numerical models to quantify the uncertainty and its impact and to assist decision making under uncertainty.

The dynamics of a power grid is governed by a set of nonlinear differential algebraic equations (DAEs) [1]. The fluctuations, induced by renewable sources, are usually modeled as random input parameters with distribution and correlation function obtained from the observed or modeled data. Monte Carlo simulations (MCS) are one of the most commonly used approaches for solving stochastic DAEs. The MCS method is both robust and easy to implement, but it has a slow convergence rate, especially for computing higher statistical moments or the tails of the distributions. Recently, stochastic finite element (SFE) methods have been applied for solving the stochastic DAEs of power grids [12, 13, 26, 19]. Under certain conditions, the SFE methods present a good alternative to the MCS method in terms of computational efficiency. In SFE, the system's random input parameters are represented via truncated Karhunen–Loève expansions with a finite set of random variables. The number of said random variables, and the computational cost of SFE methods, increases with the decreasing correlation time of the input random processes. If the correlation time is large relative to the characteristic time of the system, the random inputs can be treated as random constants and hence represented by a single random variable. In this case, the SFE methods present an excellent alternative to MCS. On the other hand, for random parameters with small correlation lengths, the number of random variables may be large enough so that the SFE methods could incur higher computational cost than that of MCS.

Since both MCS and SFE approaches exhibit lower convergence rates for higher order of statistical moments of the state variables, they are primarily used to compute the mean and variance. Furthermore, SFE methods based on generalized polynomial chaos (gPC) expansions might not converge at all for higher moments [6]. The mean gives an unbiased estimation of the most probable response of a system, while the variance is a measure of uncertainty associated with such a prediction. In many applications, including risk analysis and decision making under uncertainty, the knowledge of the first two moments may be insufficient. Instead, one may need to know the joint probability density function (PDF) of state variables. In the special case of uncorrelated random parameters (white noise), the PDF of stochastic ordinary differential equations (SODEs) can be described with the classical Fokker–Planck equation (FPE). Though conceptual frameworks [8, 10, 11, 20, 27, 30] have been proposed in physics literature for nonzero correlation lengths (colored noise), they usually require the noise to have a specific correlation structure and/or one-point distribution. Random parameters can be treated as uncorrelated if their correlation lengths/times are smaller than the time-step required to resolve the system's dynamics, and such treatment has been used in the past for renewable energy modeling (wind power [18, 23], solar power [24]). Wind speed measurements indicate that the correlation time of wind speed is of the same order as the characteristic (relaxation) time of wind generators. It has also been shown that SODEs with white noise are inadequate for accurate description of other engineered and natural systems.

Recently, we proposed a PDF method for Langevin equations with colored noise [32]. In this paper, we apply the PDF framework to derive deterministic equations for the joint PDF for a system of SODEs describing dynamics of a power generator with time-correlated input parameters. In section 2 a brief mathematical formulation of the problem is provided. In section 3 we introduce the PDF method for the SODEs and derive a deterministic PDF

equation for the joint PDF of phase angle and speed. Numerical solutions of the PDF equation are presented and compared with the results of MCS in section 4. Conclusions are given in section 5.

2. Problem formulation. We consider a simple power system consisting of a single generator and an infinite bus. The electromechanical behavior of this system can be described by the following set of ordinary differential equations (ODEs) [1]:

$$\frac{\mathrm{d}\theta}{\mathrm{d}t} = \omega_{\mathrm{B}}(\omega - \omega_{\mathrm{s}}), \tag{2.1a}$$

$$\frac{\mathrm{d}\omega}{\mathrm{d}t} = \frac{\omega_{\mathrm{s}}}{2H}\left[P_{\mathrm{m}} - P_{\mathrm{e}} - D\left(\omega - \omega_{\mathrm{s}}\right)\right], \tag{2.1b}$$

where the state variables are the phase angle $\theta \in [0, 2\pi)$ between the axis of the generator and the magnetic field and the generator angular speed $\omega \in (-\infty, \infty)$. The generator has inertia H, internal voltage E, base speed ω_{B}, and synchronization speed ω_{s}; the bus has voltage V, the generator supplies electric power P_{e} to the infinite bus, and the system has total reactance X. Additionally, the damping factor D is introduced to ensure the stability of the system.

The generator electrical power is given by the algebraic relation in terms of θ and the various voltages,

$$P_{\mathrm{e}} = \frac{EV}{X}\sin\theta. \tag{2.2}$$

For general power systems, the voltage V can be a function of the phase angles given by a set of algebraic constraints so that one obtains a set of differential algebraic equations (DAEs) governing the electromechanical behavior of the system.

The generator has a "renewable" power input $P_{\mathrm{m}}(t)$, which is modeled as a stochastic time process characterized by its mean $\langle P_{\mathrm{m}}\rangle > 0$, variance σ^2, and correlation function $\rho(t, s, \lambda)$ with correlation time λ,

$$\langle P'_{\mathrm{m}}(t)P'_{\mathrm{m}}(s)\rangle = \sigma^2\rho(t, s, \lambda), \tag{2.3}$$

where $P_{\mathrm{m}} = \langle P_{\mathrm{m}}\rangle + P'_{\mathrm{m}}$, and P'_{m} is the process's zero-mean fluctuation.

In the following, we substitute (2.2) into (2.1b) to obtain the ODEs

$$\frac{\mathrm{d}\theta}{\mathrm{d}t} = \omega_{\mathrm{B}}(\omega - \omega_{\mathrm{s}}), \tag{2.4a}$$

$$\frac{\mathrm{d}\omega}{\mathrm{d}t} = \frac{\omega_{\mathrm{s}}}{2H}\left[P_{\mathrm{m}} - P_{\max}\sin\theta - D\left(\omega - \omega_{\mathrm{s}}\right)\right], \tag{2.4b}$$

subject to the initial conditions

$$\theta(t = 0) = \theta_0, \quad \omega(t = 0) = \omega_0, \tag{2.5}$$

where $P_{\max} = EV/X$.

3. PDF method.

3.1. PDF formulation. Mechanical power $P_{\mathrm{m}}(t)$ from renewable sources typically exhibits random variability in time. Combined with potential uncertainty from initial system states, any prediction of the system's electromechanical behavior (2.4) is rendered uncertain. Our goal here is to derive a closed-form computable equation for the joint PDF of angle and speed, $p(\Theta, \Omega; t)$, for (2.4) with P_m having an arbitrary correlation function ρ and nonzero correlation time λ. To do so, we employ the PDF method originally developed in the context of turbulent flows [4] and later extended for advective-reactive transport in porous media [29] and general Langevin equations [32].

We start by introducing the "raw" (or "fine-grained") PDF of system state (θ, ω) at time t,

$$\Pi(\Theta, \Omega; t) = \delta[\theta(t) - \Theta]\, \delta[\omega(t) - \Omega]. \tag{3.1}$$

Here, $0 \le \Theta < 2\pi$ and $-\infty < \Omega < \infty$ are variables covering the outcome space of the random quantities $\theta(t)$ and $\omega(t)$, respectively.

By construction, the ensemble average of Π over all possible realizations of (θ, ω) at time t yields the joint PDF of θ and ω:

$$\langle \Pi(\Theta, \Omega; t) \rangle \equiv \iint_A \delta(\theta' - \Theta)\delta(\omega' - \Omega)\, p(\theta', \omega'; t)\, \mathrm{d}\theta' \mathrm{d}\omega' = p(\Theta, \Omega; t), \tag{3.2}$$

where $A = [0, 2\pi) \cup (-\infty, +\infty)$ is the outcome space.

In Appendix A, we show that $\Pi(\Theta, \Omega; t)$ obeys the first-order hyperbolic partial differential equation (PDE)

$$\frac{\partial \Pi}{\partial t} + \nabla_{\mathbf{x}} \cdot (\mathbf{v}\Pi) = 0, \tag{3.3a}$$

where $\mathbf{x} = (\Theta, \Omega)^{\top}$, $\nabla_{\mathbf{x}} = (\partial/\partial\Theta, \partial/\partial\Omega)^{\mathrm{T}}$. The stochastic drift "velocity" $\mathbf{v}(\mathbf{x})$ is given by

$$\mathbf{v}(\mathbf{x}) = \left[\omega_{\mathrm{B}}(\Omega - \omega_{\mathrm{s}}),\ \frac{\omega_{\mathrm{s}}}{2H}\left\{P_{\mathrm{m}} - P_{\max}\sin\Theta - D(\Omega - \omega_{\mathrm{s}})\right\}\right]^{\mathrm{T}}. \tag{3.3b}$$

The initial condition for (3.3a) corresponds to that of the swing equation (2.4):

$$\Pi(\Theta, \Omega; t = 0) = \delta(\theta_0 - \Theta)\, \delta(\omega_0 - \Omega). \tag{3.4}$$

Furthermore, we impose periodic boundary conditions on the Θ direction and vanishing boundary conditions on the Ω direction:

$$\Pi(\Theta + 2\pi,\ \Omega;\ t) \ = \ \Pi(\Theta,\ \Omega;\ t); \tag{3.5a}$$

$$\Pi(\Theta,\ \Omega = \pm\infty;\ t) = \ 0. \tag{3.5b}$$

Representing the random fields Π and $\mathbf{v}$ in (3.3) as sums of their ensemble means and respective zero-mean fluctuations, and taking the ensemble average of (3.3), we obtain the equation for p,

$$\frac{\partial p}{\partial t} + \nabla_{\mathbf{x}} \cdot (\langle \mathbf{v} \rangle p) = -\frac{\partial}{\partial \Omega}\langle P'_{\mathrm{m}} \Pi' \rangle, \tag{3.6}$$

where the mean advective velocity $\langle \mathbf{v}(\mathbf{x}) \rangle$ is given by

$$\langle \mathbf{v} \rangle(\mathbf{x}) = \left[\omega_{\mathrm{B}}(\Omega - \omega_{\mathrm{s}}),\ \frac{\omega_{\mathrm{s}}}{2H} \left\{ \langle P_{\mathrm{m}} \rangle - P_{\max} \sin\Theta - D(\Omega - \omega_{\mathrm{s}}) \right\} \right]^{\mathrm{T}}. \tag{3.7}$$

Equation (3.6) contains the cross-covariance term $\langle P'_{\mathrm{m}} \Pi' \rangle$, which cannot be computed exactly without solving the original stochastic ODEs (2.4). In the following section we propose a large-eddy-diffusivity closure for $\langle P'_{\mathrm{m}} \Pi' \rangle$.

3.2. Large-eddy-diffusivity closure. To obtain a closed-form PDF equation, we employ a closure scheme—variously known as the large-eddy-diffusivity (LED) closure [16] or the weak approximation [22]—which has been previously used in stochastic averaging of advective transport of a passive scalar in random velocity fields [29, 31, 32, 33, 34]. In contrast to existing LED closures and the weak approximation, our proposed closure allows us to capture the effect of nonzero correlation times in the cross-covariance term $\langle P'_{\mathrm{m}} \Pi' \rangle$ for systems described by a velocity field $\mathbf{v}(\mathbf{x})$ of nonzero divergence.

The derivations of the PDF equation are given in Appendix B, and its final form is

$$\frac{\partial p}{\partial t} + \nabla_{\mathbf{x}} \cdot (\langle \mathbf{v} \rangle p) = \frac{\partial}{\partial \Omega} \left\{ \boldsymbol{\mathcal{D}} \nabla_{\mathbf{x}} p \right\}, \tag{3.8}$$

where the "eddy-diffusivity" (second-rank) tensor $\boldsymbol{\mathcal{D}}$ has the nonzero components

$$\mathcal{D}_{\Omega\Omega}(\mathbf{x}, t) = \frac{\omega_s^2}{4H^2} \int_0^t \langle P'_{\mathrm{m}}(t) P'_{\mathrm{m}}(s) \rangle \frac{\partial \Omega}{\partial \tilde{\Omega}(s|\mathbf{x}, t)} \mathrm{d}s, \tag{3.9a}$$

$$\mathcal{D}_{\Omega\Theta}(\mathbf{x}, t) = \frac{\omega_s^2}{4H^2} \int_0^t \langle P'_{\mathrm{m}}(t) P'_{\mathrm{m}}(s) \rangle \frac{\partial \Theta}{\partial \tilde{\Omega}(s|\mathbf{x}, t)} \mathrm{d}s. \tag{3.9b}$$

In (3.9), $\boldsymbol{\chi}(s|\mathbf{x}, t) = (\tilde{\Theta}(s|\mathbf{x}, t), \tilde{\Omega}(s|\mathbf{x}, t))^{\top}$ denotes the Lagrangian coordinate at time s, defined as the solution at time s of the ODE

$$\frac{\mathrm{d}\boldsymbol{\chi}(s'|\mathbf{x}, t)}{\mathrm{d}s'} = \langle \mathbf{v}(\boldsymbol{\chi}(s'|\mathbf{x}, t), s') \rangle, \quad s' \in [s, t], \tag{3.10}$$

with terminal condition $\boldsymbol{\chi}(t|\mathbf{x}, t) = \mathbf{x}$, where $\mathbf{x}$ is the Eulerian coordinate.

Boundary conditions of the joint PDF equation (3.8) are obtained by taking the ensemble average of (3.5):

$$p(\Theta + 2\pi, \Omega; t) = p(\Theta, \Omega; t); \tag{3.11a}$$

$$p(\Theta, \Omega = \pm\infty; t) = 0. \tag{3.11b}$$

Similarly, given the SODE (2.4) with deterministic initial conditions (2.5), the corresponding initial condition for the PDF equation is

$$p(\Theta, \Omega; t = 0) = \delta(\theta_0 - \Theta)\, \delta(\omega_0 - \Omega). \tag{3.12}$$

Equation (3.8), together with the diffusion tensor (3.9), forms a conservation law and therefore satisfies both a strong maximum and a strong minimum principle. Given the initial

condition (3.12), it is guaranteed that the solution of (3.8), (3.11)–(3.12) is nonnegative for any $t > 0$ given that $p(\mathbf{x}, 0) \geq 0$. Similarly, being governed by a conservation law, it follows from $\int_A p(\mathbf{x}, 0)\, \mathrm{d}\mathbf{x} = 1$ that the PDF integrates to one for any $t > 0$.

Compared to standard practices described in the introduction, the formulation of the PDF equation of (3.8) offers a number of advantages. Unlike the Fokker–Planck equation (FPE), the PDF method is applicable to SODEs driven by noise with arbitrary stationary or nonstationary correlation structure and nonzero correlation length. Also, the derivation of the PDF equation imposes no assumptions on the one-point PDF of the noise P'_{m}. The PDF equation is linear, which facilitates the analytical and numerical analysis of (nonlinear) SODEs. Last and most importantly, by going beyond conventional mean and variance, the PDF equation provides a full one-point stochastic characterization of system states, including one-point statistics of arbitrary order and probabilities of rare events, useful for probabilistic risk assessment.

The proposed LED closure is distinguished from classical LED closures [16, 22] by the appearance of the terms $\partial\Omega/\partial\Omega'(s|\mathbf{x}, t)$ and $\partial\Theta/\partial\Omega'(s|\mathbf{x}, t)$ in (3.9). These terms capture the effect of the divergence of the stochastic drift velocity in the diffusion tensor, which plays an important role starting at second order of the correlation time. If these terms were not considered, the element $\mathcal{D}_{\Omega\Theta}$ of the diffusion tensor would be neglected, leading to an inaccurate approximation of the dynamics of the PDF.

The damping factor in (2.4) induces the damping rate $\gamma = D\omega_{\mathrm{s}}/2H$. In Appendix C, we demonstrate that for correlation times shorter than the relaxation time-scale γ^{-1}, i.e., for $\lambda D\omega_{\mathrm{s}}/2H \ll 1$, the components of the diffusion tensor can be approximated as

$$\mathcal{D}_{\Omega\Omega}(\mathbf{x}, t) = \frac{\omega_{\mathrm{s}}^2}{4H^2} \int_0^t \left\langle P'_{\mathrm{m}}(t) P'_{\mathrm{m}}(t-\tau) \right\rangle \left(1 - \tau \frac{D\omega_{\mathrm{s}}}{2H}\right) \mathrm{d}\tau, \tag{3.13a}$$

$$D_{\Omega\Theta}(\mathbf{x}, t) = \frac{\omega_{\mathrm{s}}^2}{4H^2} \int_0^t \left\langle P'_{\mathrm{m}}(t) P'_{\mathrm{m}}(t-\tau) \right\rangle \tau\omega_{\mathrm{B}}\, \mathrm{d}\tau. \tag{3.13b}$$

For the particular case of the exponential correlation function

$$\left\langle P'_{\mathrm{m}}(t) P'_{\mathrm{m}}(t-\tau) \right\rangle = \sigma^2 \exp\left\{-|\tau|/\lambda\right\},$$

we can evaluate the integrals in (3.13) analytically, obtaining

$$\mathcal{D}_{\Omega\Omega}(t) = \frac{\sigma^2\omega_{\mathrm{s}}^2}{4H^2} \left[\lambda(1 - e^{-t/\lambda}) + \frac{D\omega_{\mathrm{s}}}{2H}\lambda \left\{te^{-t/\lambda} - \lambda(1 - e^{-t/\lambda})\right\}\right], \tag{3.14a}$$

$$\mathcal{D}_{\Omega\Theta}(t) = \frac{\sigma^2\omega_{\mathrm{s}}^2}{4H^2}\lambda\omega_{\mathrm{B}} \left\{\lambda(1 - e^{-t/\lambda}) - te^{-t/\lambda}\right\}. \tag{3.14b}$$

Disregarding transients, these diffusion coefficients simplify to

$$\mathcal{D}_{\Omega\Omega} = \frac{\sigma^2\omega_{\mathrm{s}}^2}{4H^2}\lambda \left(1 - \lambda\frac{D\omega_{\mathrm{s}}}{2H}\right), \quad \mathcal{D}_{\Omega\Theta} = \frac{\sigma^2\omega_{\mathrm{s}}^2}{4H^2}\lambda^2\omega_{\mathrm{B}}. \tag{3.15}$$

3.3. Comparison against the FPE. It is interesting to evaluate how the PDF equation obtained via the proposed LED closure compares against the FPE corresponding to a white

noise approximation of the zero-mean fluctuation P'_{m}. It has been noted that the classical LED closure is consistent with the FPE [30, 31]. In this section we assess the consistency of the proposed LED closure.

In the white noise approximation, we replace the colored fluctuation with a Gaussian noise process of correlation structure $\langle P'_{\mathrm{m}}(t)P'_{\mathrm{m}}(t-\tau)\rangle = \sigma^2\lambda\delta(\tau)$. For such a process, the evolution of the PDF is given exactly by the FPE [27]

$$\frac{\partial p}{\partial t} + \nabla_{\mathbf{x}} \cdot (\langle \mathbf{v}\rangle p) = \lambda \frac{\sigma^2\omega_{\mathrm{s}}^2}{4H^2}\frac{\partial^2}{\partial\Omega^2}p.$$

Comparing the diffusion coefficients of the FPE to the diffusion coefficients of (3.15), we can see that the white noise approximation is a first-order in λ approximation of the correct behavior of the PDF. For small but nontrivial correlation times, the white noise approximation overestimates the diffusion coefficient $\mathcal{D}_{\Omega\Omega}$ by a factor of approximately $1 + \lambda D\omega_{\mathrm{s}}/2H$ and thus overestimates the uncertainty of the process driven by colored noise.

It is important to point out that for the white noise correlation structure, the coefficients of the LED diffusion tensor (3.9) reduce to

$$\mathcal{D}_{\Omega\Omega} = \lambda\frac{\sigma^2\omega_{\mathrm{s}}^2}{4H^2}, \quad \mathcal{D}_{\Omega\Theta} = 0,$$

which shows that the proposed LED closure is exact for Gaussian white noise.

3.4. Numerical implementation. Various approaches have been proposed for the numerical solution of the FPE and similar equations (see, e.g, [5, 27]). In the following computational examples, we solve the PDF equation (3.8) numerically using a flux-based finite difference (FD) scheme for spatial discretization. In this scheme, discrete values in each grid point $\mathbf{x}_i = (\Theta_i, \Omega_i)^\top$ represent the average solution of $p_i = p(\mathbf{x}_i, t)$ in a cell of size $\Delta\Theta\Delta\Omega$ centered around $\mathbf{x}_i$. To prevent numerical diffusion due to discretization of the advection term, and to avoid nonlinear instabilities due to sharp solution gradients, we adopt a nonlinear fifth-order essentially nonoscillatory scheme [14]. For time discretization, we use the strong-stability-preserving (SSP) Runge–Kutta (RK) scheme [28]. The resulting system of linear equations is solved using the high-performance numerical library PETSc [2, 3].

4. Computational example. We solve the PDF equation (3.8) with the diffusion coefficient (3.14). We assume that $P'_{\mathrm{m}}(t)$ has zero mean, variance σ^2, and an exponential correlation function with correlation time λ, $\langle P'_{\mathrm{m}}(t)P'_{\mathrm{m}}(t-\tau)\rangle = \sigma^2\exp\{-|\tau|/\lambda\}$.

The PDF equation is solved subject to the initial condition

$$p(\Theta, \Omega; t = 0) = \delta(\theta_{\mathrm{eq}} - \Theta)\,\delta(\omega_{\mathrm{eq}} - \Omega), \tag{4.1}$$

where θ_{eq} and ω_{eq} are the steady state operation (or nominal) values of the phase angle and angular speed. In steady state operation, the angular speed is equal to the synchronization speed, and the average mechanical power input $\langle P_{\mathrm{m}}\rangle$ is equal to the electrical power output $P_{\max}\sin\theta$, or

$$\theta_{\mathrm{eq}} = \arcsin\langle P_{\mathrm{m}}\rangle/P_{\max}, \quad \omega_{\mathrm{eq}} = \omega_{\mathrm{s}}. \tag{4.2}$$

In the first computational example, we set the values of the system's parameters to $P_{\max} = 2.1$, $H = 5$, $D = 5$, and $\omega_{\mathrm{B}} = 120\pi$, typical of power systems [17]. For the stochastic mechanical power input, we choose its average as $\langle P_{\mathrm{m}} \rangle = 0.9$ and standard deviation $\sigma = 0.1$ so that the generator is operated in steady state equilibrium at a nominal angle θ_{eq} well below $\pi/2$ (the point of instability for the system (2.4)) and the phase angle has an adequate margin to oscillate and return to its nominal angle.

The FD grid is chosen so that $\mathbf{x}_{\mathrm{eq}} = (\theta_{\mathrm{eq}}, \omega_{\mathrm{eq}})^\top$ is a grid point. Numerically, the Dirac delta initial condition (4.1) is implemented as $p_i = 1/(\Delta\Theta\Delta\Omega)$ for $\mathbf{x}_i = \mathbf{x}_{\mathrm{eq}}$ and zero otherwise, which is mass-equivalent to the Dirac delta for the grid average FD formulation employed.

Finally, we use the correlation time $\lambda = 10/\omega_B \approx 0.0265$, chosen to be smaller than the damping time-scale but nontrivial.

A set of Monte Carlo simulations (MCS) is also conducted to validate the PDF method. The SDEs (2.4) are integrated numerically using a second-order strong RK scheme [21], together with an evolution equation for the Ornstein–Uhlenbeck (O–U) process that generates the exponentially correlated Gaussian fluctuations P'_{m}. The initial value of P'_{m} is drawn directly from the stationary Gaussian distribution of the O–U process. The time-step Δt satisfies $\Delta t \leq \lambda/5$ in order to sufficiently resolve variations in P'_{m}.

Figure 1 shows the comparison of the marginal PDFs $p_\theta(\Theta, t)$ and $p_\omega(\Omega, t)$,

$$p_\theta(\Theta, t) = \int_{-\infty}^{\infty} p(\Theta, \Omega; t)\, \mathrm{d}\Omega, \quad p_\omega(\Omega, t) = \int_0^{2\pi} p(\Theta, \Omega; t)\, \mathrm{d}\Theta, \tag{4.3}$$

obtained from the PDF equation (3.8) with diffusion coefficient (3.14), and MCS. This figure shows the marginal PDFs at the times $t = 0.5$, $t = 1.0$, and $t = 5.0$. The comparison shows good agreement between the PDF solutions and MCS.

Figures 2 and 3 present various temporal snapshots of the marginal PDFs p_θ and p_ω, together with 50 realizations of the solution to the SDEs (2.4), illustrating the convergence of the marginal PDFs to their steady state counterparts, and the evolution of the system towards stochastic stationarity. It can be seen that the PDFs widen with time, i.e., uncertainty in the rotational speed and angle increases, and eventually approach steady state configurations. The steady state coefficient of variance (CV) of angle ($\sigma_\theta/\langle\theta\rangle = 0.2217$) is two orders of magnitude larger than the CV of speed ($\sigma_\omega/\langle\omega\rangle = 0.0023$); i.e., there is significantly more uncertainty in the prediction of θ than in that of ω.

4.1. Effect of correlation time. According to (3.9), the correlation time λ impacts the evolution of p_θ and p_ω through the LED dispersion coefficient $\boldsymbol{\mathcal{D}}$. Figure 4 shows p_θ and p_ω for three values of the correlation time: $\lambda = 5 \times 10^{-4}$, $\lambda = 5 \times 10^{-3}$, and $\lambda = 5 \times 10^{-2}$. In Figure 4, the marginal PDFs are presented at time $t = 1.0$.

It follows from (3.14) that $\mathcal{D}_{\Omega\Omega}$ and $\mathcal{D}_{\Omega\Theta}$ are functions of the correlation time. They are both equal to zero for $\lambda = 0$ and grow with increasing λ for $\lambda D\omega_{\mathrm{s}}/H < 1$. For $\lambda D\omega_{\mathrm{s}}/H > 1$, $\mathcal{D}_{\Omega\Omega}$ decreases, and $\mathcal{D}_{\Omega\Theta}$ keeps increasing quadratically with λ. As a consequence, the variance of the joint PDFs increases with increasing λ for the values of λ considered, as can be seen in Figure 4. It can be seen that the computed marginal PDFs agree well with their MCS counterparts.

The approximated diffusion coefficients (3.14) are valid only for correlation times shorter

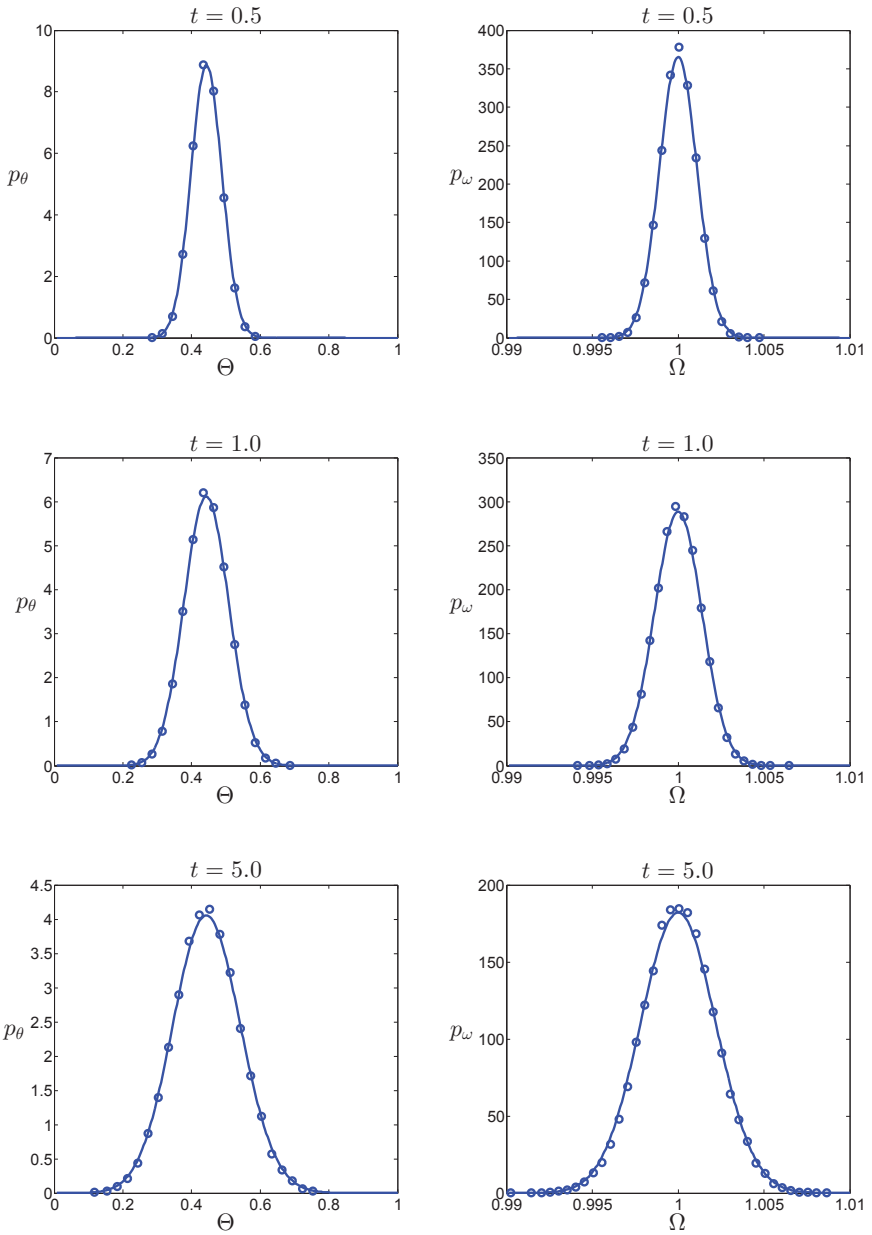

Figure 1. *Marginal PDFs* Θ *and* Ω *computed using MCS and the PETSc solver of the PDF equation* (3.8) *at times* $t = 0.5$, 1.0, *and* 5.0. *(—) PETSc, (∘) MCS. Results are obtained for* $P_{\max} = 2.1$, $H = 5$, $D = 5$, $\omega_{\mathrm{B}} = 120\pi$, $\langle P_{\mathrm{m}} \rangle = 0.9$, $\sigma = 0.1$, *and* $\lambda = 10/\omega_{\mathrm{B}}$.

than the relaxation time-scale. As the correlation time approaches, and exceeds, the relaxation time-scale, we expect the approximated diffusion coefficients to become progressively less accurate and eventually nonphysical. It is therefore expected that the PDFs computed via the PDF equation would be less accurate with respect to MCS as the correlation time

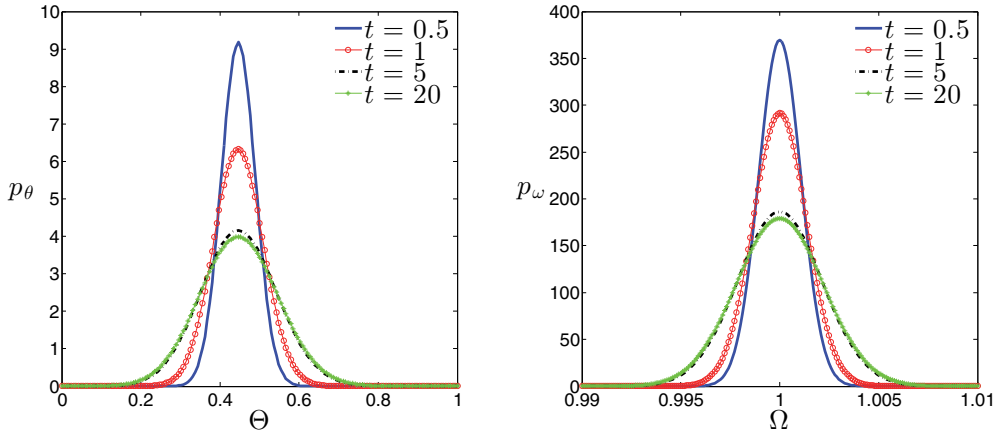

Figure 2. *Temporal snapshots of the marginal PDFs (left) $p_\theta(\Theta, t)$ and (right) $p_\omega(\Omega, t)$ computed from (3.8) at times $t = 0.5$, 1, 5, and 20. Results are obtained for $P_{\max} = 2.1$, $H = 5$, $D = 5$, $\omega_B = 120\pi$, $\langle P_m \rangle = 0.9$, $\sigma = 0.1$, and $\lambda = 10/\omega_B$.*

increases. Such an effect would be strongly noticeable at the stationary state. We numerically verify this behavior in Figure 5, where we present stationary marginal PDFs computed for $\lambda = 10/\omega_B$, $20/\omega_B$, and $50/\omega_B$. It can be seen that as the correlation time increases, the computed marginal PDFs progressively deviate from their MCS counterparts, overestimating the uncertainty of both phase angle and angular speed.

Nevertheless, we can derive a PDF equation accurate for very long correlation times by employing a dimension reduction argument. For very long but finite λ, we observe that the angular speed stabilizes to the deterministic value ω_s over the correlation time-span, while the phase angle stabilizes to an uncertain value $\theta \approx \arcsin P_m/P_{\max}$. Over multiple correlation time-spans, the behavior of the system is thus approximately overdamped, so that we may disregard the inertia term $d\omega/dt$ in (2.4), effectively removing the angular speed variable and reducing the problem to a single Langevin equation for $\theta(t)$.

In Appendix D, we show that the resulting approximate equation governing the marginal PDF p_θ is

$$\frac{D}{\omega_B}\frac{\partial p_\theta}{\partial t} + \frac{\partial}{\partial \Theta}\left[(\langle P_m \rangle - P_{\max}\sin\Theta)\, p_\theta\right] = \frac{\partial^2}{\partial \Theta^2}\left\{\mathcal{D}_{\Theta\Theta}(\Theta, t) p_\theta\right\}, \tag{4.4}$$

where the inhomogeneous coefficient $\mathcal{D}_{\Theta\Theta}$ (not a diffusion coefficient) is given by

$$\mathcal{D}_{\Theta\Theta} = \frac{\omega_B}{D}\frac{\lambda\sigma^2}{1 + \lambda\omega_B P_{\max}\cos\Theta/D}\left\{1 - \exp\left(-\frac{\lambda t}{1 + \lambda\omega_B P_{\max}\cos\Theta/D}\right)\right\}. \tag{4.5}$$

The marginal PDF of the angular speed is $p_\omega = \delta(\Omega - \omega_s)$.

We recover a transport equation by approximating $\cos\Theta$ in (4.5) with $\cos\theta_{eq}$. The stationary solution of this equation in the limit $\lambda \to \infty$ is shown in Figure 6. It can be seen that it compares favorably with the corresponding MCS, computed for $\lambda = 1 \times 10^5/\omega_B$.

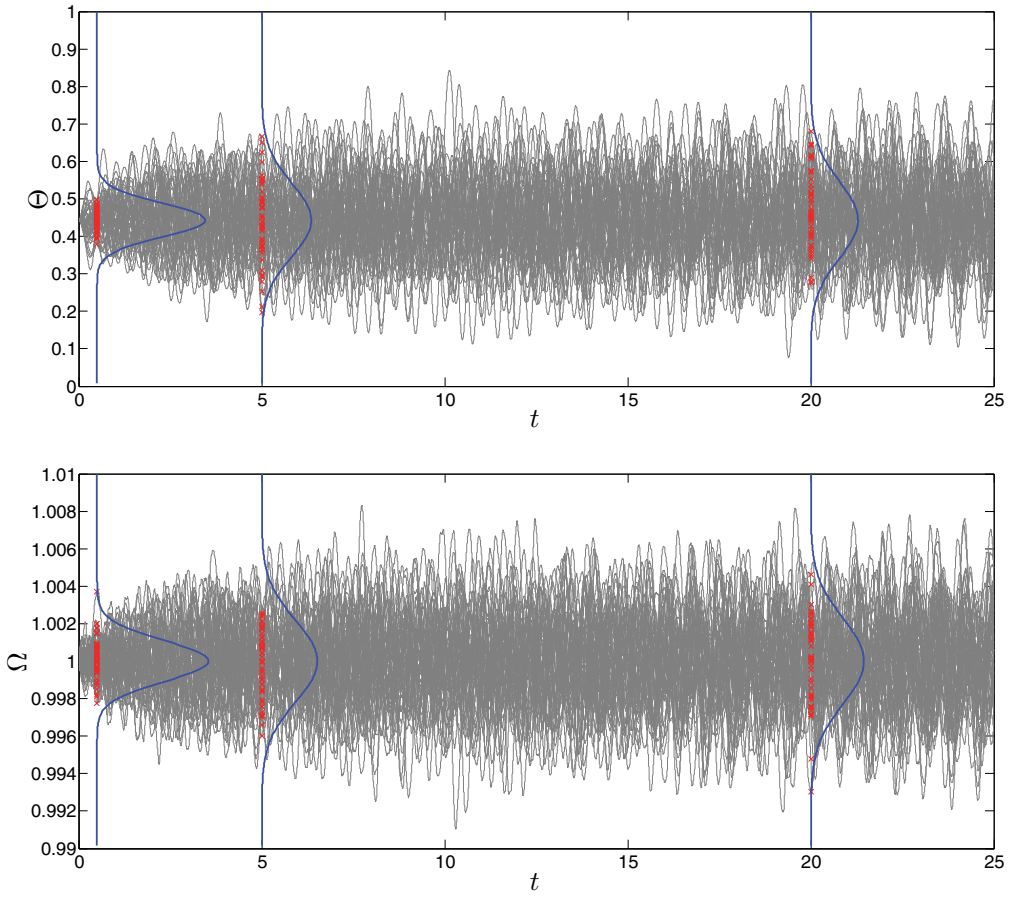

Figure 3. *Realizations of the solution to the SDEs (2.4) and temporal snapshots of the marginal PDFs computed at times $t = 0.5$, 5, and 20. Results are obtained for $P_{\max} = 2.1$, $H = 5$, $D = 5$, $\omega_B = 120\pi$, $\langle P_m \rangle = 0.9$, $\sigma = 0.1$, and $\lambda = 10/\omega_B$.*

4.2. Effects of variance of P_m. Uncertainty of the mechanical input P_m is characterized by its variance σ^2. Figure 7 shows the effect of σ^2 on the marginal PDFs. In this figure, the marginal PDFs are shown for $\sigma^2 = 1 \times 10^{-4}$, $\sigma^2 = 1 \times 10^{-3}$, and $\sigma^2 = 1 \times 10^{-2}$ at time $t = 1.0$. As expected, increasing σ^2 leads to widening of the marginal PDFs.

Figure 8 illustrates the stochastic behavior of the system for $\sigma^2 = 0.25$ and $\sigma^2 = 1.0$, which are an order of magnitude larger than the largest variance used in the simulations in Figure 7. It can be seen that for these large values of σ^2 the stationary marginal distribution of the phase angle is approximately uniformly distributed over the support $[0, 2\pi)$, as opposed to the unimodal behavior centered around θ_{eq} that is observed for the smaller variances. The shifted stationary marginal distribution of the angular speed in Figure 8 indicates that for large variance the generator rotates with a speed different from the synchronization speed ω_s. The PDFs computed for the large variance scenarios compare favorably with their MCS counterparts, indicating that the LED closure remains accurate for large variances in the

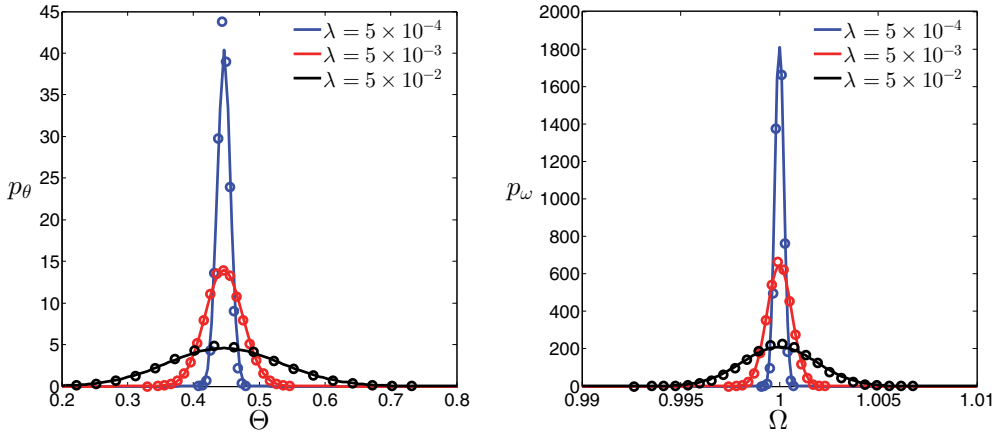

Figure 4. *Snapshots of the marginal PDFs (left) $p_\theta(\Theta, t = 1)$ and (right) $p_\omega(\Omega, t = 1)$ for $\lambda = 5 \times 10^{-4}$, 5×10^{-3}, and 5×10^{-2}. (—) PETSc, (∘) MCS. Results are obtained for $P_{\max} = 2.1$, $H = 5$, $D = 5$, $\omega_B = 120\pi$, $\langle P_m \rangle = 0.9$, and $\sigma = 0.1$.*

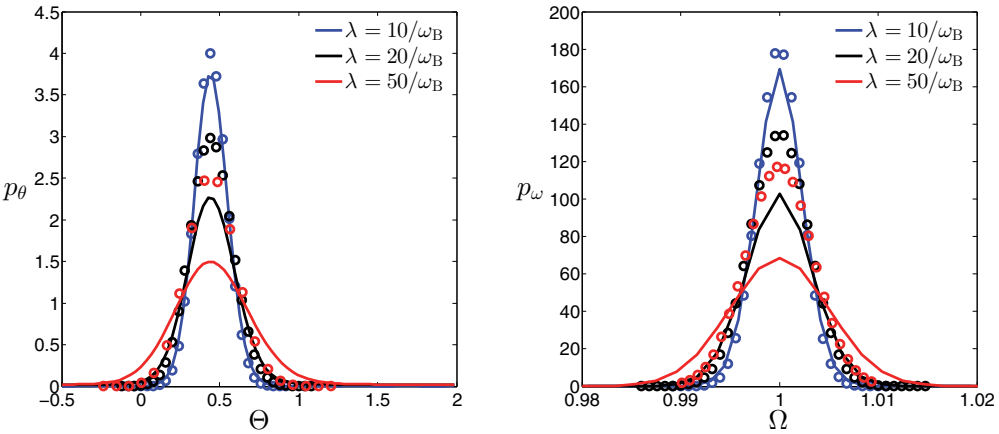

Figure 5. *Stationary PDFs (left) $p_\theta(\Theta)$ and (right) $p_\omega(\Omega)$ for $\lambda = 10/\omega_B$, $20/\omega_B$, and $50/\omega_B$. (—) PETSc, (∘) MCS. Results are obtained for $P_{\max} = 2.1$, $H = 5$, $D = 5$, $\omega_B = 120\pi$, $\langle P_m \rangle = 0.9$, and $\sigma = 0.1$.*

Gaussian noise case.

4.3. Effect of damping coefficient D. Here we consider the effect of a damping coefficient on the solution of the PDF equation subject to the equilibrium initial condition for a system with parameters $\sigma^2 = 0.01$, $P_{\max} = 2.1$, $H = 5$, $\omega_B = 120\pi$, and $\langle P_m \rangle = 0.9$.

Figure 9 shows the mean and variance of θ and ω versus time for $D = 0$, 5, and 50. The mean and variance were found from the solution of the PDF equation by computing the moment integrals $\langle \theta \rangle = \int_0^{2\pi} \Theta p_\theta(\Theta) d\Theta$, $\sigma_\theta^2 = \int_0^{2\pi} (\Theta - \langle \theta \rangle)^2 p_\theta(\Theta) d\Theta$, $\langle \omega \rangle = \int_{-\infty}^{\infty} \Omega p_\omega(\Omega) d\Omega$, and $\sigma_\omega^2 = \int_{-\infty}^{\infty} (\Omega - \langle \omega \rangle)^2 p_\omega(\Omega) d\Omega$. It can be seen that for $D \neq 0$, $\langle \theta \rangle$ nonmonotonically approaches an asymptotic value that depends on D. For $D = 0$, $\langle \theta \rangle$ is a nonmonotonic function that diverges for $t \to \infty$, indicating that the system eventually operates outside the

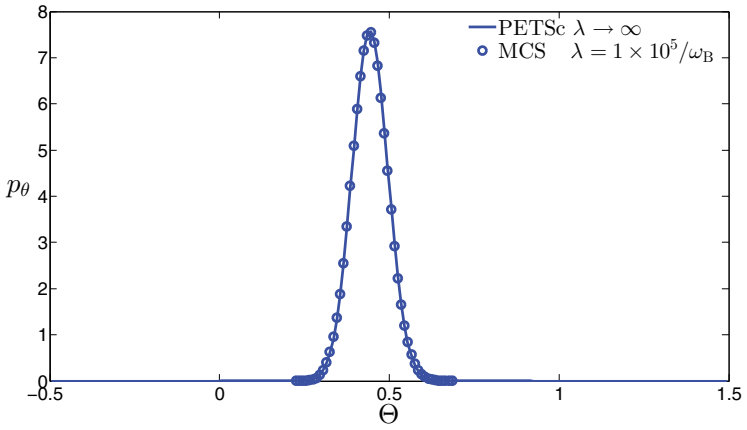

Figure 6. *Stationary PDF $p_\theta(\Theta)$ for $\lambda \to \infty$ (PETSc) and $\lambda = 1 \times 10^5/\omega_B$ (MCS). Results are obtained for $P_{max} = 2.1$, $H = 5$, $D = 5$, $\omega_B = 120\pi$, $\langle P_m \rangle = 0.9$, and $\sigma = 0.1$.*

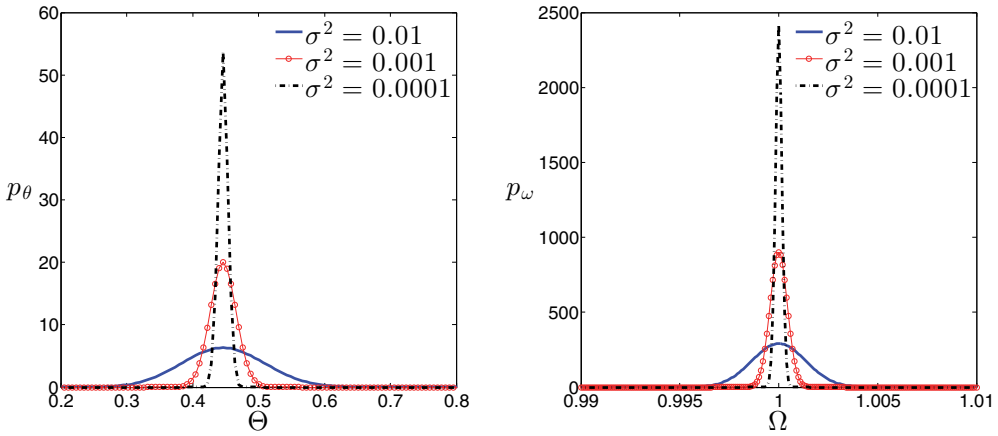

Figure 7. *Snapshots of marginal PDFs (left) $p_\theta(\Theta, t = 1)$ and (right) $p_\omega(\Omega, t = 1)$ for $\sigma^2 = 1 \times 10^{-4}$, 1×10^{-3}, and 1×10^{-2}. Results are obtained for $P_{max} = 2.1$, $H = 5$, $D = 5$, $\omega_B = 120\pi$, $\langle P_m \rangle = 0.9$, and $\lambda = 10/\omega_B$.*

originating period $[0, 2\pi)$ and moves to subsequent ones. For $D \neq 0$, $\langle \omega \rangle$ nonmonotonically decreases to ω_{eq}, while for $D = 0$ $\langle \omega \rangle$ it oscillates around ω_{eq}. For $D \neq 0$, the variances of θ and ω monotonically increase to asymptotic values dependent on D. For $D = 0$, both σ_θ^2 and σ_ω^2 diverge for $t \to \infty$. These results indicate that for the PDF equation to have a steady state solution, the damping coefficient should be greater than zero.

4.4. Effects of nonequilibrium initial conditions. In the above scenarios, we used the equilibrium initial conditions and found that for sufficiently small σ and large D, $\langle \omega \rangle$ and $\langle \theta \rangle$ (the centers of mass of the marginal PDFs) stay at their respective equilibrium values throughout the simulation. In this section we consider the effect of nonequilibrium initial conditions on the joint and marginal PDFs of θ and ω. Specifically, we solve the PDF equation

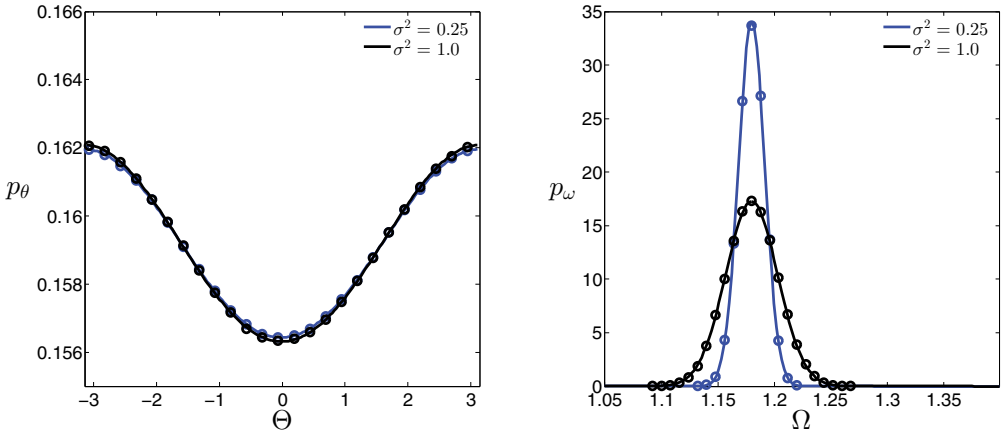

Figure 8. *Stationary marginal PDFs (left) $p_\theta(\Theta)$ and (right) $p_\omega(\Omega)$ for $\sigma^2 = 0.25$ and 1.0. (—) PETSc, (○) MCS. Results are obtained for $P_{\max} = 2.1$, $H = 5$, $D = 5$, $\omega_B = 120\pi$, $\langle P_m \rangle = 0.9$, and $\lambda = 10/\omega_B$.*

subject to the nonequilibrium initial condition (3.12) with $\theta_0 = 0.89\theta_{eq}$ and $\omega_0 = 0.99\omega_{eq}$ and two damping coefficients, $D = 0$ (Figure 10) and $D = 50$ (Figure 11).

Figure 10 shows a set of temporal snapshots of the joint PDF p, marginal PDFs, and means $\langle\theta\rangle$ and $\langle\omega\rangle$ for the simulation with $D = 0$. We can see that $\langle\theta\rangle$ and $\langle\omega\rangle$ oscillate around the corresponding equilibrium values, while the overall predictive uncertainty (width of the PDFs) increases with time. In the simulation with strong damping ($D = 50$, Figure 11), $\langle\theta\rangle$ and $\langle\omega\rangle$ oscillate but converge to their equilibrium values. The joint and marginal PDFs initially widen but approach steady state values with time. These figures also show a good agreement between the PDFs found from the solution of the PDF equation and MCS.

Although not presented in this work, similar behavior of the PDF equation is observed for other nonequilibrium initial conditions, namely ($\theta_0 = 0.89\theta_{eq}$, $\omega_0 = 1.01\omega_s$), ($\theta_0 = 1.11\theta_{eq}$, $\omega_0 = 0.99\omega_s$), and ($\theta_0 = 1.11\theta_{eq}$, $\omega_{in} = 1.01\omega_s$).

5. Conclusion.

We presented the PDF method for the SODEs describing the dynamics of a generator with uncertain power input. The uncertain power input is treated as a stochastic time-correlated process with a known covariance function. We used the PDF method in combination with the LED closure to obtain a deterministic equation for the joint PDF of the generator phase angle and angular speed of a generator. We solved the resulting equation numerically. The accuracy of the LED closure and numerical solutions was verified via comparison with MCS.

Our analysis leads to the following conclusions:

1. Good agreement with MCS shows that the PDF method in combination with the LED closure gives an accurate estimate of the PDFs of the system states for the various cases studied.

2. The resultant PDFs of phase angle and angular speed enable one to compute the probability of rare events, which is of particular interest to power system design and reliability analysis. For example, it enables one to choose the damping coefficient D so as to keep ω and θ within design range of values with the desired probability.

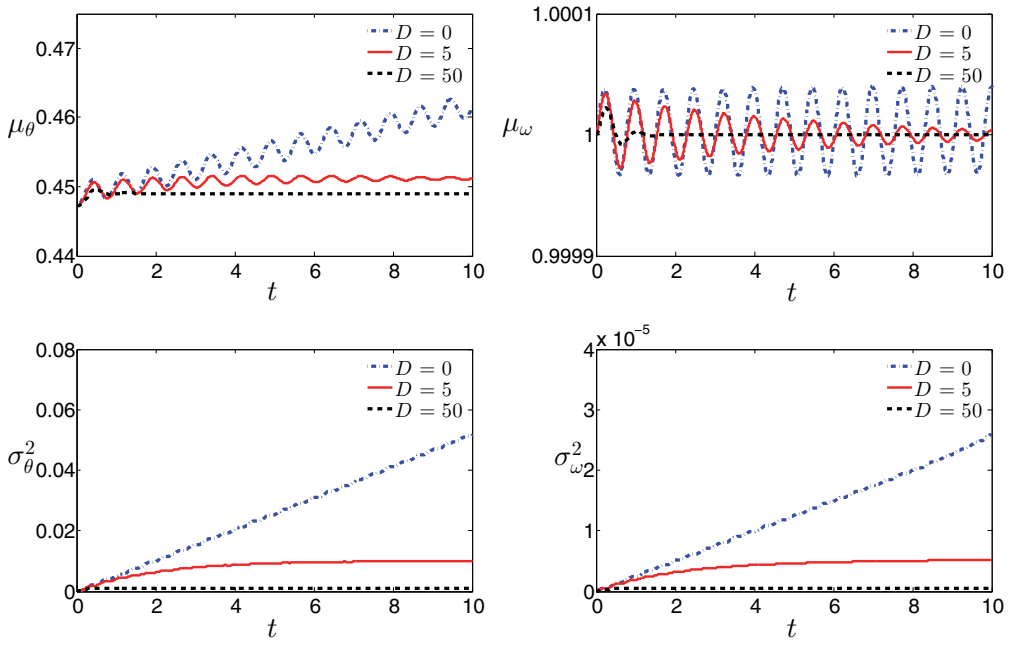

Figure 9. *Mean and variance of θ and ω as a function of time for $D = 0$, $D = 5$, and $D = 50$. Results are obtained for $P_{\max} = 2.1$, $H = 5$, $\omega_B = 120\pi$, $\langle P_m \rangle = 0.9$, $\sigma = 0.01$, and $\lambda = 10/\omega_B$.*

3. Unlike most of the existing methods for deriving PDF equations for Langevin equations, the proposed PDF method allows one to write a closed-form PDE equation for the PDF of a system of stochastic ODEs such as (2.4) without any restriction on the correlation structure of the noise terms and for nonzero correlation times.

4. The LED closure in the derivations of the PDF equation does not require any assumptions on the distribution of uncertain input signals. We demonstrated that for autocorrelated fluctuations the PDFs obtained with the LED approximation agree well with the MCS. By comparison with the corresponding FPE, we demonstrated that the LED approximation is exact for delta-correlated Gaussian fluctuations.

5. The derivation of PDF equations can be easily extended to power grid systems with multiple generators by using the presented LED closure. While other closures have been proposed for single Langevin equations or Kramers equations which cover a wider range of correlation times (see [7, 9]), our approach is distinguished by its weak assumptions and straightforward extensibility. The extension of the LED closure to higher powers of the correlation time is the topic of ongoing research.

6. It is observed that the system exhibits unimodal stochastic behavior when the standard deviation σ of the power input fluctuations is small with respect to the peak electrical power $P_{\max}$ and the damping factor D is sufficiently large. Under such conditions, the stationary average angular speed $\langle \omega \rangle$ is equal to the synchronization speed ω_s. When σ is of the same order of magnitude of $P_{\max}$, the system switches to operation conditions with $\langle \omega_s \rangle \neq \omega_s$.

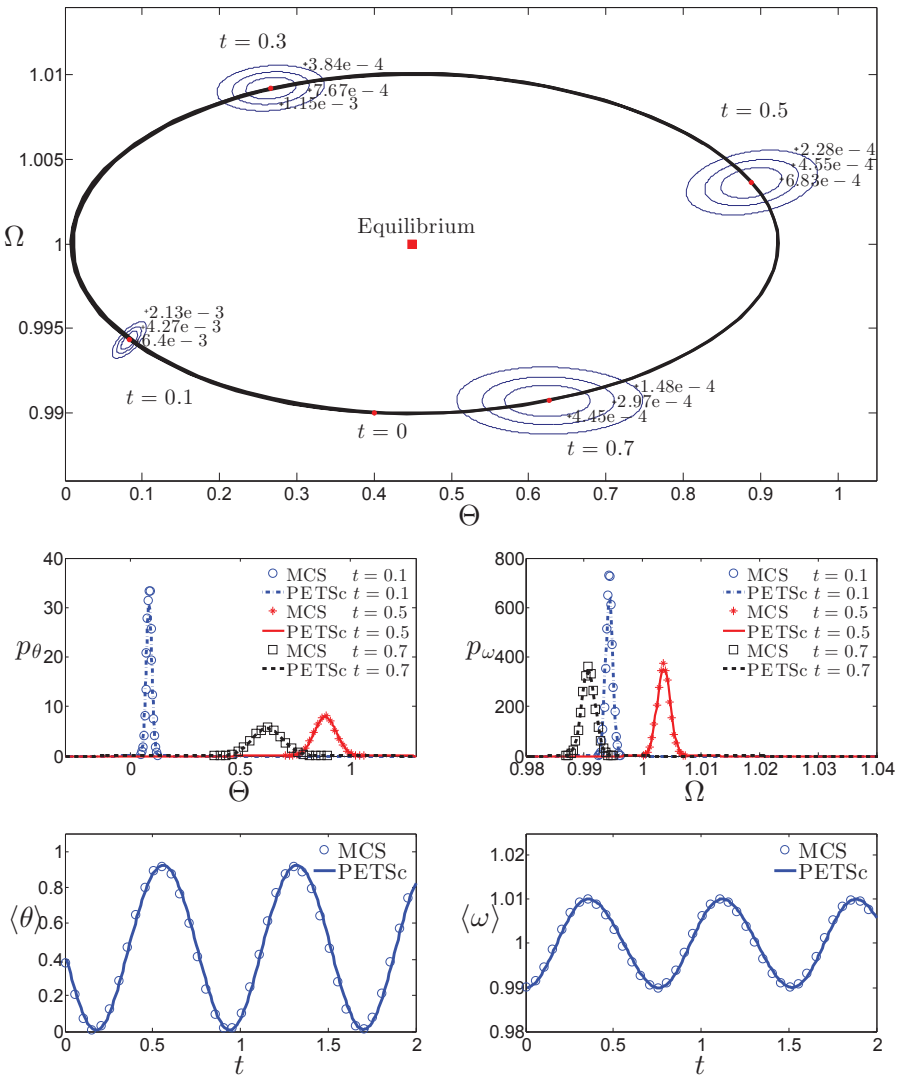

Figure 10. *Dynamics of stochastic system with nonequilibrium initial condition* (3.12), $\theta_0 = 0.89\theta_{\rm eq}$, *and* $\omega_0 = 0.99\omega_{\rm eq}$ *and damping coefficient* $D = 0$. *(Top) joint PDF at times* $t = 0$, 0.1, 0.3, 0.5, *and* 0.7, *along with the trajectory of* $\langle\theta\rangle$ *and* $\langle\omega\rangle$ *(the equilibrium point* $(\theta_{\rm eq}, \omega_{\rm eq})$ *is marked by the red square); (middle) snapshots of the marginal PDFs* p_θ *and* p_ω *computed using MCS and the PETSc solver of the PDF equation; (bottom) temporal evolution of* $\langle\theta\rangle$ *and* $\langle\omega\rangle$. *Results are obtained for* $P_{\max} = 2.1$, $H = 5$, $\omega_{\rm B} = 120\pi$, $\langle P_{\rm m}\rangle = 0.9$, $\sigma = 0.1$, *and* $\lambda = 10/\omega_{\rm B}$.

Appendix A. Derivation of stochastic equation for raw PDF. Following the derivation of PDF equations for transport of a scalar in a turbulent velocity field [25] and randomly heterogeneous porous media [29], the partial derivative in time of the raw PDF Π is given by

$$\frac{\partial \Pi}{\partial t} = -\frac{\partial \Pi}{\partial \Theta}\frac{\mathrm{d}\theta}{\mathrm{d}t} - \frac{\partial \Pi}{\partial \Omega}\frac{\mathrm{d}\omega}{\mathrm{d}t}. \tag{A.1}$$

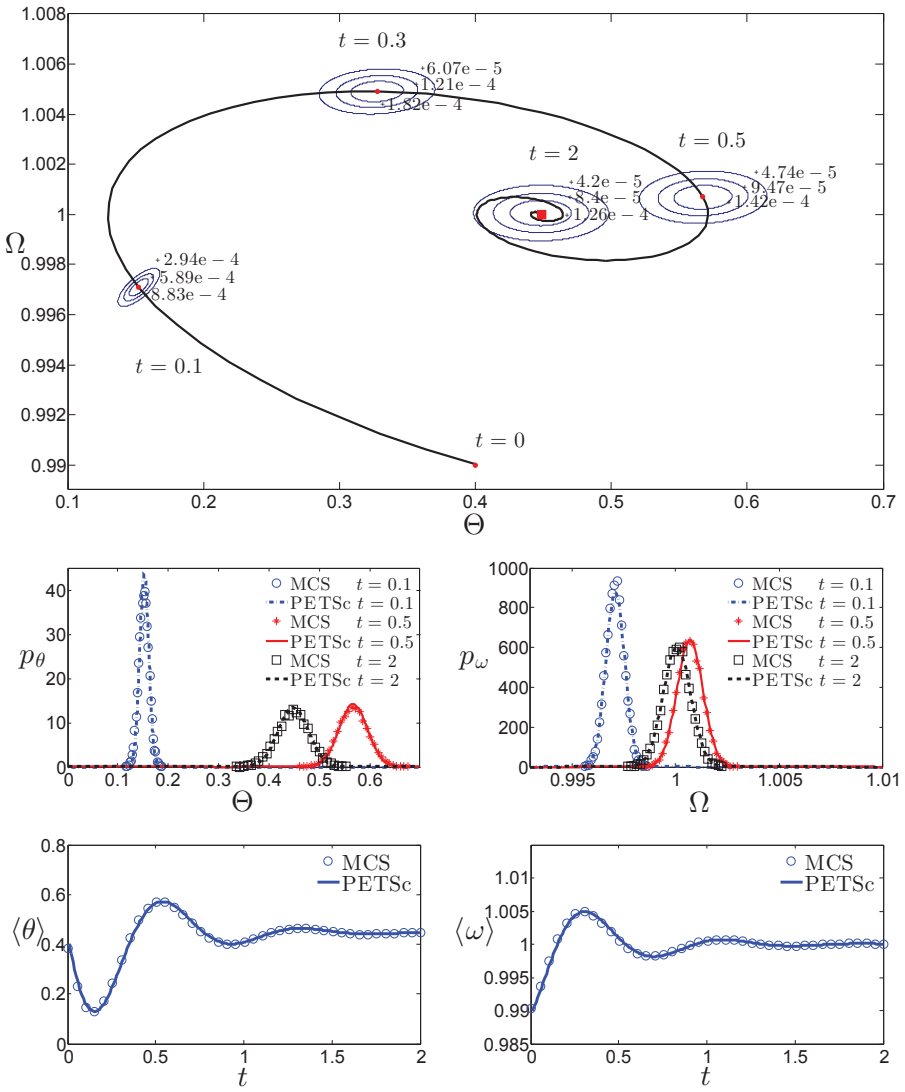

Figure 11. *Dynamics of stochastic system with nonequilibrium initial condition* (3.12), $\theta_0 = 0.89\theta_{\rm eq}$, *and* $\omega_0 = 0.99\omega_{\rm eq}$ *and damping coefficient* $D = 50$. *(Top) joint PDF at times* $t = 0$, 0.1, 0.3, 0.5, *and* 0.7, *along with the trajectory of* $\langle\theta\rangle$ *and* $\langle\omega\rangle$ *(the equilibrium point* $(\theta_{\rm eq}, \omega_{\rm eq})$ *is marked by the red square); (middle) snapshots of the marginal PDFs* p_θ *and* p_ω *computed using MCS and the PETSc solver of the PDF equation; (bottom) temporal evolution of* $\langle\theta\rangle$ *and* $\langle\omega\rangle$. *Results are obtained for* $P_{\max} = 2.1$, $H = 5$, $\omega_{\rm B} = 120\pi$, $\langle P_{\rm m}\rangle = 0.9$, $\sigma = 0.1$, *and* $\lambda = 10/\omega_{\rm B}$.

Multiplying (2.4a) and (2.4b) by $\partial\Pi/\partial\Omega$ and $\partial\Pi/\partial\Theta$, respectively, yields

$$\frac{\partial\Pi}{\partial\Theta}\frac{\mathrm{d}\theta}{\mathrm{d}t} = \frac{\partial}{\partial\Theta}\left[\Pi\,\omega_{\rm B}(\omega-\omega_{\rm s})\right], \tag{A.2a}$$

$$\frac{\partial\Pi}{\partial\Omega}\frac{\mathrm{d}\omega}{\mathrm{d}t} = \frac{\partial}{\partial\Omega}\left\{\Pi\frac{\omega_{\rm s}}{2H}\left[P_{\rm m} - P_{\max}\sin\theta - D(\omega-\omega_{\rm s})\right]\right\}. \tag{A.2b}$$

Invoking the shifting property of the Dirac-delta function, $g(\theta)\delta(\theta-\Theta)=g(\Theta)\delta(\theta-\Theta)$, we rewrite (A.2a) and (A.2b) as

$$\frac{\mathrm{d}\theta}{\mathrm{d}t}\frac{\partial\Pi}{\partial\Theta}=\frac{\partial}{\partial\Theta}\left[\Pi\,\omega_{\mathrm{B}}(\Omega-\omega_{\mathrm{s}})\right], \tag{A.3a}$$

$$\frac{\mathrm{d}\omega}{\mathrm{d}t}\frac{\partial\Pi}{\partial\Omega}=\frac{\partial}{\partial\Omega}\left\{\Pi\frac{\omega_{\mathrm{s}}}{2H}\left[P_{\mathrm{m}}-P_{\max}\sin\Theta-D(\Omega-\omega_{\mathrm{s}})\right]\right\}. \tag{A.3b}$$

Substituting (A.3a)–(A.3b) into (A.1) we obtain the stochastic equation (3.3) governing Π.

Appendix B. LED approximation. An equation for the fluctuation of the raw PDF, $\Pi'=\Pi-p$, is obtained by subtracting (3.6) from (3.3a):

$$\frac{\partial\Pi'}{\partial t}+\nabla_{\mathbf{x}}\cdot(\langle\mathbf{v}\rangle\Pi')=-\nabla_{\mathbf{x}}\cdot(\mathbf{v}'\Pi-\langle\mathbf{v}'\Pi'\rangle). \tag{B.1}$$

Next, we introduce the Green's function $G(\mathbf{x},t|\mathbf{y},s)$ associated with the first-order hyperbolic operator in (B.1), satisfying the equation

$$\frac{\partial G}{\partial s}+\langle\mathbf{v}\rangle\cdot\nabla_{\mathbf{y}}G=-\delta(\mathbf{x}-\mathbf{y})\delta(t-s),\quad s\in(0,t), \tag{B.2}$$

and subject to the homogeneous terminal condition $G(\mathbf{x},t|\mathbf{y},t)=0$ and boundary conditions

$$G(\mathbf{x},t|\Theta',\Omega',s)=G(\mathbf{x},t|\Theta'+2\pi,\Omega',s);\quad G(\mathbf{x},t|\Theta',\Omega'\pm\infty,s)=0. \tag{B.3}$$

In (B.1) we replace $(\mathbf{x},t)$ with $(\mathbf{y},s)$, multiply times $G(\mathbf{x},t|\mathbf{y},s)$, and integrate over the outcome space A and time domain, yielding

$$\int_0^t\iint_A G\left[\frac{\partial\Pi'}{\partial s}+\nabla_{\mathbf{y}}\cdot(\langle\mathbf{v}\rangle\Pi')\right]\mathrm{d}\mathbf{y}\,\mathrm{d}s=-\int_0^t\iint_A G\nabla_{\mathbf{y}}\cdot(\mathbf{v}'\Pi-\langle\mathbf{v}'\Pi'\rangle)\,\mathrm{d}\mathbf{y}\,\mathrm{d}s. \tag{B.4}$$

Integrating by parts, the left-hand side of (B.4) leads to

$$\begin{aligned}&\iint_A\left[G\Pi'\right]_{s=0}^{s=t}\mathrm{d}\mathbf{y}+\int_0^t\iint_{\partial A}\mathbf{n}\cdot\mathbf{v}\Pi' G\,\mathrm{d}\mathbf{y}\,\mathrm{d}s-\int_0^t\iint_A\Pi'\left\{\frac{\partial G}{\partial s}+\nabla_{\mathbf{y}}\cdot(\langle\mathbf{v}\rangle G)\right\}\mathrm{d}\mathbf{y}\,\mathrm{d}s\\&\qquad=-\int_0^t\iint_A G\nabla_{\mathbf{y}}\cdot(\mathbf{v}'\Pi-\langle\mathbf{v}'\Pi'\rangle)\,\mathrm{d}\mathbf{y}\,\mathrm{d}s,\end{aligned} \tag{B.5}$$

where $\mathbf{n}$ denotes the outward vector normal to the boundary of A, ∂A.

We now invoke the boundary conditions for p (3.11) and Π (3.5), and compute their counterparts for $\Pi'=\Pi-p$, from which we can see that the second integral on the left-hand side of (B.5) vanishes identically. Substituting (B.2) into (B.5), employing the initial condition for the Green's function, and denoting by $\mathbf{Q}$ the cross-correlation $\langle\mathbf{v}'\Pi'\rangle$, we obtain

$$\Pi'=-\int_0^t\iint_A G\nabla_{\mathbf{y}}\cdot(\mathbf{v}'\Pi-\mathbf{Q})\,\mathrm{d}\mathbf{y}\,\mathrm{d}s+\iint_A G\Pi'|_{s=t}\,\mathrm{d}\mathbf{y}. \tag{B.6}$$

The second term in the right-hand side of (B.6) vanishes identically if the initial conditions of the SODE system are deterministic.

Multiplying (B.6) times $\mathbf{v}'(\mathbf{x},t)$ and taking the ensemble average, we obtain the following integral equation for the vector $\mathbf{Q}$:

$$\mathbf{Q}(\mathbf{x},t) = -\int_0^t \iint_A G(\mathbf{x},t|\mathbf{y},s)\left\langle \mathbf{v}'(\mathbf{x},t)\,\nabla_{\mathbf{y}}\cdot\left(\mathbf{v}'(\mathbf{y},s)\,\Pi(\mathbf{y},s)\right)\right\rangle \,\mathrm{d}\mathbf{y}\,\mathrm{d}s. \tag{B.7}$$

Now we have an exact (but not closed) expression for the mixed ensemble moment $\mathbf{Q}$. The LED closure consists of two steps: breaking of the averages in (B.7), and introducing a localization hypothesis. The breaking of averages consists of employing the approximation

$$\langle v_i' v_j' \Pi\rangle \approx \langle v_i' v_j'\rangle p.$$

Employing this approximation and substituting (B.7) into (3.6) we can rewrite the equation for the joint PDF as the time-convoluted integro-differential equation

$$\frac{\partial p}{\partial t} + \nabla_{\mathbf{x}}\cdot\left(\langle\mathbf{v}\rangle p + \boldsymbol{\mathcal{V}}[p]\right) = \nabla_{\mathbf{x}}\cdot\mathbf{J}[p], \tag{B.8}$$

where

$$\mathbf{J}(\mathbf{x},t) = \int_0^t \iint_A G(\mathbf{x},t|\mathbf{y},s)\langle\mathbf{v}'(\mathbf{x},t)\mathbf{v}'(\mathbf{y},s)\rangle\nabla_{\mathbf{y}}p(\mathbf{y},s)\,\mathrm{d}\mathbf{x}\,\mathrm{d}s, \tag{B.9a}$$

$$\boldsymbol{\mathcal{V}}(\mathbf{x},t) = -\int_0^t \iint_A G(\mathbf{x},t|\mathbf{y},s)\,p(\mathbf{y},s)\langle\mathbf{v}'(\mathbf{x},t)\nabla_{\mathbf{y}}\cdot\mathbf{v}'(\mathbf{y},s)\rangle\,\mathrm{d}\mathbf{y}\,\mathrm{d}s. \tag{B.9b}$$

A similar integro-differential equation was derived in [22] for the advective transport of a passive scalar in a random velocity field.

The nonlocal flux (B.9a) and nonlocal drift (B.9b) terms impose dependence on the spatio-temporal history of the joint PDF throughout the evolution of the stochastic system. To remove said dependence, a localization of the nonlocal terms must be provided.

Before introducing the localization assumption, we first need to compute the Green's function G. Let $\boldsymbol{\chi}(t'|\mathbf{x},t)$ denote the Lagrangian coordinate at time t', defined as the solution at time t' of the ODE

$$\frac{\mathrm{d}\boldsymbol{\chi}(s|\mathbf{x},t)}{\mathrm{d}s} = \langle\mathbf{v}(\boldsymbol{\chi}(s|\mathbf{x},t),s)\rangle, \tag{B.10}$$

satisfying $\boldsymbol{\chi}(t|\mathbf{x},t)=\mathbf{x}$, where $\mathbf{x}$ is the Eulerian coordinate.

The characteristics of the Green's function problem (B.2) are given by (B.10). Along said characteristics, the Green's function problem becomes

$$\frac{\mathrm{d}}{\mathrm{d}s'}G(\mathbf{x},t|\boldsymbol{\chi}(s'|\mathbf{y},s),s') = -\delta(t-s')\delta(\mathbf{x}-\boldsymbol{\chi}(s'|\mathbf{y},s)), \quad G(\mathbf{x},t|\boldsymbol{\chi}(t|\mathbf{y},s),t)=0, \quad s'\in(0,t).$$

Integrating from s to t, we obtain

$$G(\mathbf{x},t|\mathbf{y},s) = \int_s^t \delta(t-s')\delta(\mathbf{x}-\boldsymbol{\chi}(s'|\mathbf{y},s))\,\mathrm{d}s' = \mathcal{H}(t-s)\delta(\mathbf{x}-\boldsymbol{\chi}(t|\mathbf{y},s)). \tag{B.11}$$

This result allows us to evaluate integrals over the outcome space A of the Green's function times functions of $\mathbf{y}$ as follows:

$$\begin{aligned}\int_A G(\mathbf{x},t|\mathbf{y},s)f(\mathbf{y})\,\mathrm{d}\mathbf{y} &= \mathcal{H}(t-s)\int_A \delta(\mathbf{x}-\boldsymbol{\chi}(t|\mathbf{y},s))f(\mathbf{y})\,\mathrm{d}\mathbf{y}\\ &= \mathcal{H}(t-s)\int_{A'}\left|\det\frac{\partial\mathbf{y}}{\partial\boldsymbol{\chi}(t|\mathbf{y},s)}\right|\delta(\mathbf{x}-\boldsymbol{\chi}(t|\mathbf{y},s))f(\mathbf{y})\,\mathrm{d}\boldsymbol{\chi}(t|\mathbf{y},s)\\ &= \begin{cases}\mathcal{H}(t-s)\left|\det\partial\boldsymbol{\chi}(s|\mathbf{x},t)/\partial\mathbf{x}\right| f(\boldsymbol{\chi}(s|\mathbf{x},t)) & \text{if } \mathbf{x}\in A',\\ 0 & \text{if } \mathbf{x}\notin A',\end{cases}\end{aligned}$$

where $\boldsymbol{\chi}(s|\mathbf{x},t)$ is the upstream Lagrangian coordinate at time $s<t$. A' is the downstream image at time t of A at time s.

We can input (B.11) into (B.9a)–(B.9b) to obtain

$$\mathbf{J}(\mathbf{x},t)=\int_0^t\left|\det\frac{\partial\boldsymbol{\chi}(s|\mathbf{x},t)}{\partial\mathbf{x}}\right|\left\langle\mathbf{v}'(\mathbf{x},t)\mathbf{v}'(\boldsymbol{\chi}(s|\mathbf{x},t),s)\right\rangle\nabla_{\boldsymbol{\chi}}p(\boldsymbol{\chi}(s|\mathbf{x},t),s)\,\mathrm{d}s, \tag{B.12}$$

$$\boldsymbol{\mathcal{V}}(\mathbf{x},t)=-\int_0^t\left|\det\frac{\partial\boldsymbol{\chi}(s|\mathbf{x},t)}{\partial\mathbf{x}}\right|\left\langle\mathbf{v}'(\mathbf{x},t)\cdot\nabla_{\boldsymbol{\chi}}\mathbf{v}'(\boldsymbol{\chi}(s|\mathbf{x},t),s)\right\rangle p(\boldsymbol{\chi}(s|\mathbf{x},t),s)\,\mathrm{d}\tau, \tag{B.13}$$

where $\nabla_{\boldsymbol{\chi}}$ denotes the gradient with respect to $\boldsymbol{\chi}(s|\mathbf{x},t)$. Here we have assumed that $\mathbf{x}\in A'$ over the characteristic time-scale of $\langle\mathbf{v}'(\mathbf{x},t)\mathbf{v}'(\boldsymbol{\chi}(s|\mathbf{x},t),s)\rangle$, i.e., over its correlation length.

In order to deconvolve the nonlocal fluxes, we need to introduce a localization hypothesis on the joint PDF as it appears inside the integrals in (B.12)–(B.13). If the transport of probability is mostly advection-dominated, we can replace the full advection-diffusion history of p from $(\boldsymbol{\chi}(s|\mathbf{x},t),s)$ to $(\mathbf{x},t)$ with its strictly advective behavior. That is, we replace p in (B.12)–(B.13) with the solution of the problem

$$\frac{\partial p}{\partial t'}+\nabla_{\mathbf{x}}\cdot(\langle\mathbf{v}\rangle p)=0,\quad t'\in(s,t),$$

which is given in closed form as

$$p(\boldsymbol{\chi}(s|\mathbf{x},t),s)=\left|\det\frac{\partial\mathbf{x}}{\partial\boldsymbol{\chi}(s|\mathbf{x},t)}\right|p(\mathbf{x},t). \tag{B.14}$$

Plugging into (B.12)–(B.13) we obtain the localized fluxes

$$\mathbf{J}(\mathbf{x},t)=\int_0^t\left|\det\frac{\partial\boldsymbol{\chi}(s|\mathbf{x},t)}{\partial\mathbf{x}}\right|\left\langle\mathbf{v}'(\mathbf{x},t)\mathbf{v}'(\boldsymbol{\chi}(s|\mathbf{x},t),s)\right\rangle\nabla_{\boldsymbol{\chi}}\left|\det\frac{\partial\mathbf{x}}{\partial\boldsymbol{\chi}(s|\mathbf{x},t)}\right|p(\mathbf{x},t)\mathrm{d}s, \tag{B.15}$$

$$\boldsymbol{\mathcal{V}}(\mathbf{x},t)=-\int_0^t\left\langle\mathbf{v}'(\mathbf{x},t)\cdot\nabla_{\boldsymbol{\chi}}\mathbf{v}'(\boldsymbol{\chi}(s|\mathbf{x},t),s)\right\rangle p(\mathbf{x},t)\mathrm{d}s. \tag{B.16}$$

It must be noted that for systems in one dimension with $\nabla\cdot v=\partial u/\partial x=0$, the fluxes in (B.15)–(B.16) are equivalent to the localized fluxes obtained via the weak approximation [22].

For the power system (2.4), we have $\mathbf{v}'=(0,\Gamma(t))^\top$, and $|\det\partial\boldsymbol{\chi}(s|\mathbf{x},t)/\partial\mathbf{x}|=\exp\{\gamma\tau\}$, with $\Gamma(t)=P'_{\mathrm{m}}\omega_{\mathrm{s}}/2H$ and $\gamma=D\omega_{\mathrm{s}}/2H$, so that (B.15)–(B.16) simplify to

$$J_\Theta(\mathbf{x},t)=0,\quad J_\Omega(\mathbf{x},t)=-\int_0^t\langle\Gamma(t)\Gamma(s)\rangle\nabla_{\boldsymbol{\chi}}p(\mathbf{x},t)\,\mathrm{d}s,\quad \boldsymbol{\mathcal{V}}(\mathbf{x},t)=0. \tag{B.17}$$

Substituting (B.17) into (B.8) and employing the chain rule to express $\nabla_{\boldsymbol{\chi}}$ in terms of $\partial/\partial\Theta$ and $\partial/\partial\Omega$, we obtain (3.8)–(3.9).

Appendix C. Short correlation time approximation of diffusion tensor. The evaluation of the diffusion coefficient (3.9) requires the evaluation of the nonlocal terms $\partial\Omega/\partial\tilde{\Omega}(s'|\mathbf{x},t)$ and $\partial\Theta/\partial\Omega\Omega(s'|\mathbf{x},t)$ for $s' \in [s,t]$. If the correlation time of the fluctuation P'_{m} is short with respect to the relaxation time induced by the damping coefficient, i.e., if $\lambda D\omega_{\mathrm{s}}/2H \ll 1$, then it suffices to approximate these terms only for the shorter span $s' \in [t-\tau,t]$, with $\tau \ll 1$ [15].

Integrating (3.10) from $t-\tau$ to t for $\tau \ll 1$, we can write

$$\Theta = \tilde{\Theta}(t-\tau|\mathbf{x},t) + \tau\omega_B(\Omega-\omega_{\mathrm{s}}) + O(\tau^2),$$
$$\Omega = \tilde{\Omega}(t-\tau|\mathbf{x},t) + \tau\frac{\omega_{\mathrm{s}}}{2H}[\langle P_{\mathrm{m}}\rangle - P_{\mathrm{e}}(\Theta) - D(\Omega-\omega_{\mathrm{s}})] + O(\tau^2),$$

from which we obtain

$$\frac{\mathrm{d}\Theta}{\mathrm{d}\tilde{\Omega}(t-\tau|\mathbf{x},t)} = \tau\omega_{\mathrm{B}} + O(\tau^2), \quad \frac{\mathrm{d}\Omega}{\mathrm{d}\tilde{\Omega}(t-\tau|\mathbf{x},t)} = 1 - \tau\frac{D\omega_{\mathrm{s}}}{2H} + O(\tau^2). \tag{C.1}$$

Substituting into (3.9) and making the change of variables $\tau = t - s'$, we obtain (3.13).

Appendix D. PDF equation for very long correlation times. Employing the dimension reduction argument outlined in section 4.1, the system (2.4) reduces to the Langevin equation

$$\frac{D}{\omega_{\mathrm{B}}}\frac{\mathrm{d}\theta}{\mathrm{d}t} = \langle P_{\mathrm{m}}\rangle + P'_{\mathrm{m}} - P_{\max}\sin\theta. \tag{D.1}$$

The corresponding PDF equation is

$$\frac{D}{\omega_{\mathrm{B}}}\frac{\partial p_\theta}{\partial t} + \frac{\partial}{\partial\Theta}\left[(\langle P_{\mathrm{m}}\rangle - P_{\max}\sin\Theta)\,p\right] = \frac{\partial}{\partial\Theta}J_\Theta, \tag{D.2}$$

with the localized flux J_Θ (B.15) given by

$$J_\Theta = \frac{\omega_{\mathrm{B}}}{D}\int_0^t \langle P'_{\mathrm{m}}(t)P'_{\mathrm{m}}(s)\rangle \frac{\partial\Theta'(s|\Theta,t)}{\partial\Theta}\frac{\partial}{\partial\Theta'(s|\Theta,t)}\left\{\frac{\partial\Theta}{\partial\Theta'(s|\Theta,t)}p(\Theta,t)\right\}\mathrm{d}s,$$

which by virtue of the chain rule simplifies to

$$J_\Theta = \frac{\omega_{\mathrm{B}}}{D}\frac{\partial}{\partial\Theta}\left\{p(\Theta,t)\int_0^t \langle P'_{\mathrm{m}}(t)P'_{\mathrm{m}}(s)\rangle\frac{\partial\Theta}{\partial\Theta'(s|\Theta,t)}\right\}\mathrm{d}s. \tag{D.3}$$

The Lagrangian coordinate $\Theta'(s|\Theta,t)$ is defined as the solution at time s of

$$\frac{D}{\omega_{\mathrm{B}}}\frac{\mathrm{d}}{\mathrm{d}s'}\Theta'(s'|\Theta,t) = \langle P_{\mathrm{m}}\rangle - P_{\max}\sin\Theta'(s'|\Theta,t), \quad s' \in [s,t], \tag{D.4}$$

subject to $\Theta'(t|\Theta,t) = \Theta$.

The task is to compute the term $\partial\Theta/\partial\Theta'(s|\Theta,t)$, which is in general not possible in closed form. Nevertheless, we can provide an approximation that results in a PDF equation accurate for very long correlation times. Integrating (D.4) from time s to t yields

$$\Theta = \Theta'(s|\Theta,t) + \frac{\omega_{\mathrm{B}}}{D}\int_s^t \left\{\langle P_{\mathrm{m}}\rangle - P_{\max}\sin\Theta'(s'|\Theta,t)\right\}\,\mathrm{d}s',$$

which we differentiate with respect to $\Theta'(s|\Theta,t)$ to obtain the implicit expression

$$\frac{\partial\Theta}{\partial\Theta'(s|\Theta,t)} = 1 - \frac{\omega_{\mathrm{B}}}{D}\int_s^t \frac{\partial\Theta'(s'|\Theta,t)}{\partial\Theta'(s|\Theta,t)}P_{\max}\cos\Theta'(s'|\Theta,t)\,\mathrm{d}s'. \tag{D.5}$$

By the repeated application of (D.5) we obtain the expansion

$$\frac{\partial\Theta}{\partial\Theta'(s|\Theta,t)} = 1 - \frac{\omega_{\mathrm{B}}}{D}\int_s^t P_{\max}\cos\Theta'(s'|\Theta,t)\Bigg\{1 - \frac{\omega_{\mathrm{B}}}{D}\int_s^{t-s+s'} P_{\max}\cos\Theta'(s''|\Theta,t)\Big\{1-\cdots\Big\}\mathrm{d}s''\Bigg\}\mathrm{d}s'.$$

We replace $\cos\Theta'$ inside each nested integral with $\cos\Theta$ (i.e., we linearize around time t) so that we can compute the series of integrals in closed form, resulting in the power series expansion

$$\frac{\partial\Theta}{\partial\Theta'(s|\Theta,t)} = 1 - \tau\frac{\omega_{\mathrm{B}}}{D}P_{\max}\cos\Theta + \frac{1}{2}\left(\tau\frac{\omega_{\mathrm{B}}}{D}P_{\max}\cos\Theta\right)^2 - \frac{1}{6}\left(\tau\frac{\omega_{\mathrm{B}}}{D}P_{\max}\cos\Theta\right)^3 + \cdots,$$

where $\tau = t - s$.

By a resummation of the series for all orders in τ, we obtain closed-form approximation

$$\frac{\partial\Theta}{\partial\Theta'(t-\tau|\Theta,t)} = \exp\left\{-\tau\frac{\omega_{\mathrm{B}}}{D}P_{\max}\cos\Theta\right\},$$

which we can substitute into (D.3) and (D.2) to obtain the PDF equation (4.4)–(4.5).

This linearization argument is equivalent to the local linearization (LL) approach presented for single Langevin equations driven by O-U noise in [7].

Acknowledgment. We thank Daniel M. Tartakovsky for his suggestion of expressing the fluctuation of the raw PDF in terms of the average Green's function instead of the stochastic Green's function.

REFERENCES

[1] P. M. Anderson and A. A. Fouad, *Power System Control and Stability*, 2nd ed., Wiley-IEEE Press, Piscataway, NJ, 2003.

[2] S. Balay, J. Brown, K. Buschelman, V. Eijkhout, W. D. Gropp, D. Kaushik, M. G. Knepley, L. C. McInnes, B. F. Smith, and H. Zhang, *PETSc Users Manual*, Tech. Report ANL-95/11 - Revision 3.4, Argonne National Laboratory, Argonne, IL, 2013.

[3] S. Balay, J. Brown, K. Buschelman, W.D. Gropp, D. Kaushik, M. G. Knepley, L. C. McInnes, B. F. Smith, and H. Zhang, *PETSc Web Page*, http://www.mcs.anl.gov/petsc (2013).
[4] H. D. Chen, S. Y. Chen, and R. H. Kraichnan, *Probability distribution of a stochastically advected scalar field*, Phys. Rev. Lett., 63 (1989), pp. 2657–2660.
[5] H. Cho, D. Venturi, and G. E. Karniadakis, *Adaptive discontinuous Galerkin method for response-excitation PDF equations*, SIAM J. Sci. Comput., 35 (2013), pp. B890–B911.
[6] O. G. Ernst, A. Mugler, H. J. Starkloff, and E. Ullmann, *On the convergence of generalized polynomial chaos expansions*, ESAIM Math. Model. Numer. Anal., 46 (2012), pp. 317–339.
[7] S. Faetti, L. Fronzoni, P. Grigolini, and R. Mannella, *The projection approach to the Fokker-Planck equation. I. Colored Gaussian noise*, J. Statist. Phys., 52 (1988), pp. 951–978.
[8] R. F. Fox, *Functional calculus approach to stochastic differential equations*, Phys. Rev. A, 33 (1986), pp. 467–476.
[9] L. Fronzoni, P. Grigolini, P. Hanggi, F. Moss, R. Mannella, and P. V. E. McClintock, *Bistable oscillator dynamics driven by nonwhite noise*, Phys. Rev. A, 33 (1986), pp. 3320–3327.
[10] M. A. Fuentes, H. S. Wio, and R. Toral, *Effective Markovian approximation for non-Gaussian noises: A path integral approach*, Phys. A, 303 (2002), pp. 91–104.
[11] P. Hänggi and P. Jung, *Colored noise in dynamical systems*, in Advances in Chemical Physics, John Wiley & Sons, New York, 1995, pp. 239–326.
[12] J. R. Hockenberry, *Evaluation of Uncertainty in Dynamic, Reduced-Order Power System Models*, Ph.D. thesis, Massachusetts Institute of Technology, Cambridge, MA, 2000.
[13] J. R. Hockenberry and B. C. Lesieutre, *Evaluation of uncertainty in dynamic simulations of power system models: The probabilistic collocation method*, IEEE Trans. Power Syst., 19 (2004), pp. 1483–1491.
[14] G. S. Jiang and C. W. Shu, *Efficient implementation of weighted ENO schemes*, J. Comput. Phys., 126 (1996), pp. 202–228.
[15] N. G. Van Kampen, *Stochastic differential equations*, Phys. Rep., 24 (1976), pp. 171–228.
[16] R. H. Kraichnan, *Eddy viscosity and diffusivity: Exact formulas and approximations*, Complex Systems, 1 (1987), pp. 805–820.
[17] P. Kundur, N. J. Balu, and M. G. Lauby, *Power System Stability and Control*, Vol. 7, McGraw–Hill, New York, 1994.
[18] A. P. Leite, C. L. T. Borges, and D. M. Falcão, *Probabilistic wind farms generation model for reliability studies applied to Brazilian sites*, IEEE Trans. Power Syst., 21 (2006), pp. 1493–1501.
[19] G. Lin, M. Elizondo, S. Lu, and X. Wan, *Uncertainty quantification in dynamic simulations of large-scale power system models using the high-order probabilistic collocation method on sparse grids*, Int. J. Uncertain. Quantif., 4 (2014), pp. 185–204.
[20] K. Lindenberg and B. J. West, *The Nonequilibrium Statistical Mechanics of Open and Closed Systems*, VCH, New York, 1990.
[21] G. N. Milshtein and M. V. Tret'yakov, *Numerical solution of differential equations with colored noise*, J. Statist. Phys., 77 (1994), pp. 691–715.
[22] S. P. Neuman, *Eulerian-Lagrangian theory of transport in space–time nonstationary velocity fields: Exact nonlocal formalism by conditional moments and weak approximation*, Water Resour. Res., 29 (1993), pp. 633–645.
[23] G. Papaefthymiou and B. Klöckl, *MCMC for wind power simulation*, IEEE Trans. Energy Convers., 23 (2008), pp. 234–240.
[24] P. S. Perez, J. Driesen, and R. Belmans, *Characterization of the solar power impact in the grid*, in Proceedings of the International Conference on Clean Electrical Power, 2007, pp. 366–371.
[25] S. B. Pope, *Turbulent Flows*, Cambridge University Press, Cambridge, UK, 2000.
[26] P. Prempraneerach, F. S. Hover, M. S. Triantafyllou, and G. E. Karniadakis, *Uncertainty quantification in simulations of power systems: Multi-element polynomial chaos methods*, Reliab. Eng. Syst. Safe., 95 (2010), pp. 632–646.
[27] H. Risken, *The Fokker-Planck Equation: Methods of Solutions and Applications*, 2nd ed., Springer-Verlag, Berlin, 1989.
[28] C.-W. Shu and S. Osher, *Efficient implementation of essentially nonoscillatory shock capturing schemes*, J. Comput. Phys., 77 (1988), pp. 439–471.

[29] D. M. Tartakovsky and S. Broyda, *PDF equations for advective-reactive transport in heterogeneous porous media with uncertain properties*, J. Contam. Hydrol., 120-121 (2011), pp. 129–140.
[30] D. Venturi and G. E. Karniadakis, *Convolutionless Nakajima–Zwanzig equations for stochastic analysis in nonlinear dynamical systems*, Proc. R. Soc. Lond. Ser. A Math. Phys. Eng. Sci., 470 (2014), no. 2166, 20130754.
[31] D. Venturi, D. M. Tartakovsky, A. M. Tartakovsky, and G. E. Karniadakis, *Exact {PDF} equations and closure approximations for advective-reactive transport*, J. Comput. Phys., 243 (2013), pp. 323–343.
[32] P. Wang, A. M. Tartakovsky, and D. M. Tartakovsky, *Probability density function method for Langevin equations with colored noise*, Phys. Rev. Lett., 110 (2013), 140602.
[33] P. Wang and D. M. Tartakovsky, *Uncertainty quantification in kinematic-wave models*, J. Comput. Phys., 231 (2012), pp. 7868–7880.
[34] P. Wang, D. M. Tartakovsky, K. D. Jarman, Jr., and A. M. Tartakovsky, *CDF solutions of Buckley-Leverett equation with uncertain parameters*, Multiscale Model. Simul., 11 (2013), pp. 118–133.